Journal of
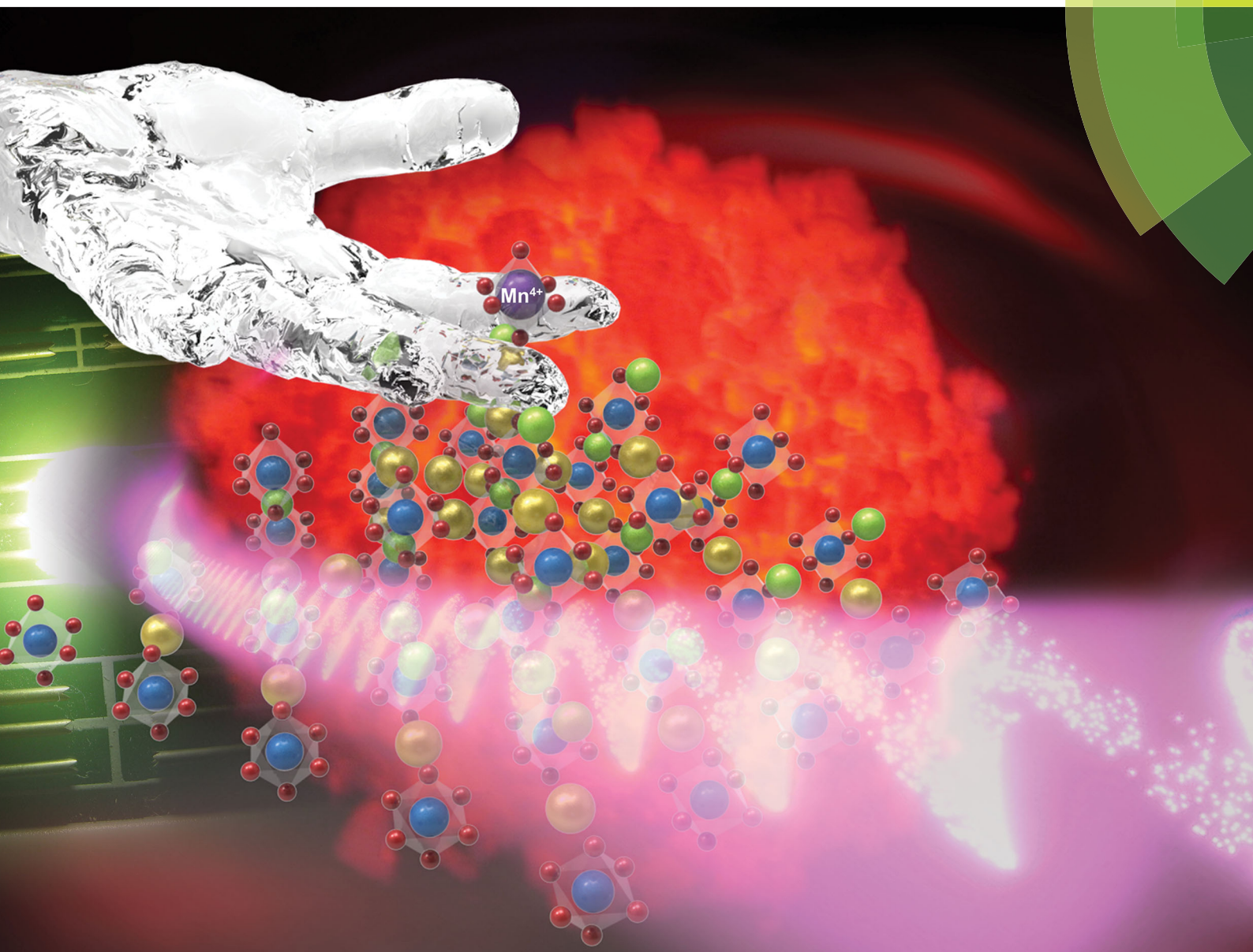# Materials Chemistry C

Materials for optical, magnetic and electronic devices

rsc.li/materials-c

PAPER
Yuexiao Pan, Jun Lin *et al.*
Room-temperature synthesis and optimized photoluminescence of a novel red phosphor NaKSnF$_6$:Mn^{4+} for application in warm WLEDs

PAPER

Room-temperature synthesis and optimized photoluminescence of a novel red phosphor NaKSnF₆:Mn⁴⁺ for application in warm WLEDs†

Luqing Xi,[a] Yuexiao Pan, [iD] *[a] Mengmeng Zhu,[a] Hongzhou Lian[b] and Jun Lin [iD] *[b]

A kind of red-emitting phosphor NaKSnF₆:Mn⁴⁺ (NKSF:Mn) has been obtained from NaF and KF with a certain molecular ratio in HF solution at room temperature. The phosphor NKSF:Mn exhibits superior optical properties including high color purity with narrow-band emissions as well as better chromaticity coordinates compared to the red phosphors Na₂SnF₆:Mn⁴⁺ (NSF:Mn) and K₂SnF₆·H₂O:Mn⁴⁺ (KSFH:Mn). The composition and structure of NKSF:Mn have been identified by X-ray diffraction (XRD), energy-dispersive X-ray spectroscopy (EDS), and transmission electron microscopy (TEM). The formation mechanism of NKSF:Mn is discussed and the morphology, thermal stability, and optical properties of NKSF:Mn have been investigated. The luminescence intensity of NKSF:Mn has been improved by optimizing synthetic parameters. A white light-emitting diode (WLED) fabricated using a blue GaN chip, a yellow YAG:Ce phosphor, and the as-prepared red phosphor NKSF:Mn exhibits superior warm white light with a color rendering index (CRI) of 90.3 at a correlated color temperature (CCT) of 3746 K.

1. Introduction

Currently, commercial white light-emitting diodes (WLEDs) based on the combination of blue-emitting GaN chips and yellow YAG:Ce phosphors provide cold white lights (CRI < 70 and CCT > 6000 K) due to the insufficiency of red components in the luminescence spectra.[1–3] A warm white light possessing a high CRI (>85) and a low CCT (3000–4500 K) is required for indoor lighting. From a practical point of view, phosphors with a broad maximum excitation band in blue, sharp emission peaks in red, and high luminescence efficiency are needed for improving the performance of WLEDs. Conventional red phosphors (such as Y₂O₃:Eu³⁺) contribute little to applications in WLEDs due to the mismatch of wavelength.[4,5]

Recently, tremendous efforts have been dedicated to the improvement of chromaticity performance of WLEDs. Red phosphors with a broad excitation band located in the blue region are mixed with YAG:Ce and coated on the chips to increase the CRI and decrease the CCT of WLEDs.[6–23] Mn⁴⁺ as a transition metal ion with outer 3d³ electron configuration shows a large gap between the energy states ⁴T₂g and ²Eg, which stabilizes the Mn⁴⁺ in the centers of octahedral sites in solid-state inorganic compounds. In these phosphors, the Mn⁴⁺ ions act as luminescence centers and are used as substitutes for Al³⁺,[6–8] Si⁴⁺,[9–13] Ti⁴⁺,[14–16] Sn⁴⁺,[17–20] Zr⁴⁺,[21,22] and Ge⁴⁺ ions in the centers of octahedra, coordinated by six O²⁻ or F⁻ ions.[6–26] So far Mn⁴⁺ ion doped luminescent materials have attracted considerable interest due to their ideal spectral characteristics for application in WLEDs as they produce narrow-band emission lines in the red region and a broad-band excitation in the blue region. For example, a high-performance WLED with CRT = 81 and CCT = 3556 K has been fabricated by a combination of red phosphor K₂TiF₆:Mn⁴⁺ with yellow YAG:Ce on blue LED chips.[14]

In general, HF and KMnO₄-rich solutions and expensive metals (such pure Ge and Zr) are needed for the synthesis of red Mn⁴⁺-doped dialkali hexafluorometallates.[22,23] So far, it has been challenging to fabricate red Mn⁴⁺ ion doped fluoride phosphors from low cost starting materials under mild reaction conditions particularly at room temperature. Mn⁴⁺-activated hexafluorostannate phosphors such as K₂SnF₆·H₂O:Mn⁴⁺, ZnSnF₆·6H₂O, Na₂SnF₆:Mn⁴⁺, and Cs₂SnF₆:Mn⁴⁺ have been synthesized by etching Sn metals in HF/KMnO₄ mixed solutions.[17–19] The practical use of previous methods has revealed several unexpected drawbacks such as the existence of crystalline water in the host lattice and contamination of MnO₂ induced by highly concentrated NaMnO₄, which are harmful to the thermal stability and

[a] Key Laboratory of Carbon Materials of Zhejiang Province, College of Chemistry and Materials Engineering, Wenzhou University, Wenzhou 325035, P. R. China. E-mail: yxpan8@gmail.com; Fax: +86-577-8837-3017; Tel: +86-577-8837-3017

[b] State Key Laboratory of Rare Earth Resource Utilization, Changchun Institute of Applied Chemistry, Chinese Academy of Sciences, Changchun 130022, P. R. China. E-mail: jlin@ciac.ac.cn, hzlian@ciac.ac.cn; Fax: +86-431-85698041; Tel: +86-431-85262031

† Electronic supplementary information (ESI) available: IR spectrum, diffuse reflectance spectra of NKSF:Mn, XRD patterns of NKSF:Mn dependent on reaction temperature and the concentration of K₂MnF₆. See DOI: 10.1039/c7tc02996a

This journal is © The Royal Society of Chemistry 2017

J. Mater. Chem. C, 2017, **5**, 9255–9263 | 9255

luminescence efficiency of the phosphors, respectively. We obtained the red phosphor NSF:Mn from metallic tin shots, NaF, and K_2MnF_6, at room temperature using a two-step method.[20] It is observed that the photoluminescence of Mn^{4+} ions is often slightly influenced by the crystallography structure, coordination environments, and remote neighbouring cations.[7,8,24] It has been reported that the photoluminescence properties (such as color purity, luminescence efficiency, and chromaticity coordinates) of K_2NaAlF_6:Mn^{4+} are much better than those of K_2LiAlF_6:Mn^{4+} due to the light nephelauxetic effect in K_2NaAlF_6.[7,8]

In the present work, we have obtained red phosphors NKSF:Mn and KSFH:Mn by a facile method including chemical etching of Sn in HF solution, anion exchange between anions $[MnF_6]^{2-}$ and $[SnF_6]^{2-}$, and recrystallization at room temperature. To our knowledge, the preparation and optical properties of Mn^{4+}-doped crystals NKSF and KSFH have not been reported so far. The photoluminescence of NKSF:Mn and KSFH:Mn is comparatively studied with that of the identified phosphor NSF:Mn. We found that the red luminescence of NKSF:Mn with ideal chromaticity coordinates and high efficiency is more favorable than those of NSF:Mn and KSFH:Mn.

2. Experimental

2.1 Synthesis of red phosphors

Materials. The raw materials were NaF (99.5%), KF (99.5%), metallic Sn (99.5%), $KMnO_4$ (AR), ethylalcohol (AR), H_2O_2 (30%) and HF (40 wt%). $KMnO_4$ and ethylalcohol were purchased from Aladdin Chemistry Co., Ltd (China). All Chemical reagents were used as received without further purification. The red phosphors NKSF:Mn, KSFH:Mn, and NSF:Mn were synthesized through a two-step chemical method.

Synthesis of host lattice compounds. 0.01 mol metallic Sn shots were dissolved completely by slowly dropping H_2O_2 in 15 mL 40 wt% HF under stirring. Then NaF and KF were added to the colorless transparent solution in a certain molecular ratio which determines the resulting products. The white powder of NKSF was produced at room temperature after stirring for 8 h. The resulting white solid compounds were filtered, washed with ethylalcohol, and dried at 60 °C for 4 h. For comparison, pure phases of KSFH and/or NSF were obtained through similar procedures in case only KF and/or NaF was provided, respectively.

Synthesis of K_2MnF_6. According to the reported procedures, 230 mmol KHF_2 and 5.7 mmol $KMnO_4$ were dissolved in 30 mL HF (40 wt%) solution, then 0.6 mL H_2O_2 (30 wt%) was added.[27] The precipitate of the K_2MnF_6 yellow powder was obtained after magnetically stirring for 30 min. The resulting yellow solid product K_2MnF_6 was collected carefully from the cup, washed extensively with ethylalcohol several times, and dried at 60 °C for 4 hours.

Synthesis of red phosphors. Red phosphors NKSF:Mn are prepared by the an anion exchange method from the as-prepared $NaKSnF_6$ and K_2MnF_6. In a typical synthesis, 0.1 mmol (0.0247 g) K_2MnF_6 was added to 20 mL of 40 wt% HF solution until

completely dissolved, and 10 mmol (2.9477 g) $NaKSnF_6$ were added to the yellow transparent solution. After magnetic stirring for 30 min, 15 mL of ethylalcohol was dropped into the mixture slowly, then the mixture was stirred for some time at room temperature. The precipitates were collected, washed with ethylalcohol several times and dried at 60 °C for 12 hours. The two red phosphors KSFH:Mn and NSF:Mn were synthesized through similar procedures.

2.2 Fabrication of LEDs using as-obtained red phosphor $NaKSnF_6$:Mn^{4+}

The as-obtained red phosphor NKSF:Mn was mixed thoroughly with commercial yellow phosphor YAG:Ce and epoxy resin in a certain proportion. The obtained mixture was coated on top of the GaN chips and dried at 130 °C for 4 hours. White lights were produced by the as-fabricated WLED devices under a driven current of 30 mA.

2.3 Characterization

XRD patterns of the products were collected on a Bruker (Karlsruhe, Germany) D8 Advance X-ray powder diffractometer (XRD) with graphite monochromated Cu Kα radiation (λ = 0.15418 nm). The XRD data were collected in the range of 10–80 degrees. The morphology and structure of the samples were studied by field emission scanning electron microscopy (FE-SEM) using a Nova NanoSEM 200 scanning electron microscope (FE-SEM, FEI Inc.) with an attached energy-dispersive X-ray spectrometer (EDS). Transmission electron microscopy (TEM) was performed on a JEOL 2100F high-resolution transmission electron microscope using an accelerating voltage of 200 kV. The thermal stability of the red phosphors is investigated by thermogravimetric (TG) analysis and differential scanning calorimetry (DSC; Netzsch STA 449 C, at a heating rate of 10 K min^{-1}). The infrared (IR) spectra were recorded on a Perkin-Elmer 580 B infrared spectrophotometer using the KBr pellet technique. UV-vis diffuse reflectance spectra were measured by using a Shimadzu UV-3600 spectrometer. Photoluminescence (PL) spectra were recorded on a FluoroMax-4 spectrofluorometer (Horiba Jobin Yvon Inc.) with a 150 W xenon lamp (as the excitation source) and a heating attachment. The internal quantum yield (QY) was measured using a barium sulfate coated integrating sphere attached to a FluoroMax-4 spectrofluorometer. The performance of WLEDs was examined using an LEE300E spectrophotocolorimeter (Everfine photo-E-Infor Co., China).

3. Results and discussion

3.1. Phase identification, morphology and composition analysis

The XRD patterns of the samples synthesized from NaF and KF with different molar ratios are shown in Fig. 1. All the samples are prepared in 40 wt% HF and all the synthetic parameters were kept identical except for the molar ratio of NaF : KF. A mixture composed of the dominant NSF (PDF NO. 41-1085) and the minor NKSF phase is obtained when the molar ratio NaF : KF is 1 : 1. With the proportion of KF increasing, the phase
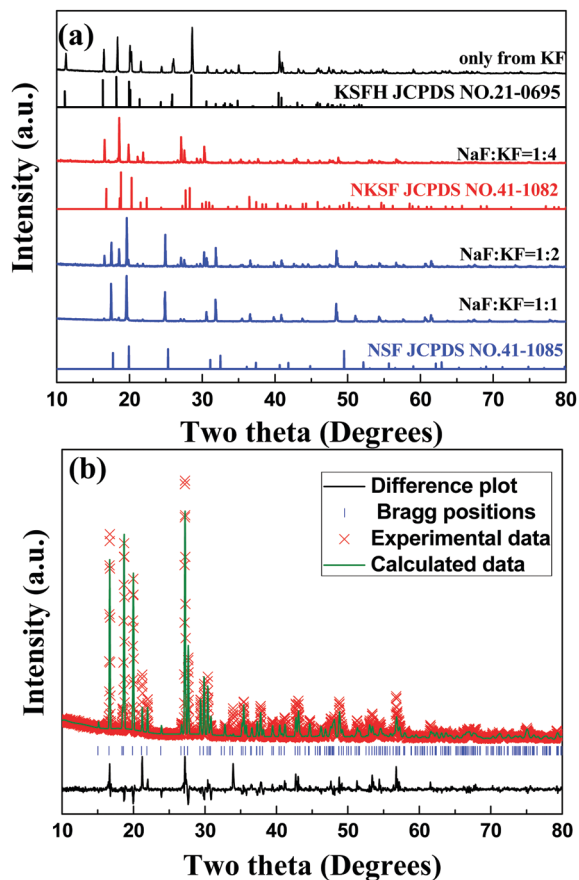
Fig. 1 (a) XRD patterns of the obtained samples prepared from NaF and KF with different molar ratios and (b) Rietveld refinement of the XRD profile of NaKSnF$_6$:Mn^{4+}.

Fig. 2 (a) XRD patterns of the samples obtained in 5–40 wt% HF solution with the mole ratio NaF : KF kept at 1 : 4. (b and c) SEM, (e) TEM images, (d) EDS spectrum, and (f) the element mapping images of Na, K, Sn, F, and Mn of selected area in the NaKSnF$_6$:Mn^{4+} sample.

of NKSF increases in the mixture and the pure NKSF is obtained when the molar ratio of NaF : KF is 1 : 4, which can be well indexed to the corresponding JCPDS card (NO. 41-1082) of NKSF. With the ratio of KF increasing further, the phase of KSFH can be detected. Pure KSFH is obtained only from KF in the absence of NaF, which is in agreement with the standard data in JCPDS card No. 21-0695. The phase transformation determined by the molar ratio of NaF and KF is attributed to the solubility of NaF (4.22 g/100 mL H$_2$O), which is much smaller than that of KF (94.9 g/100 mL H$_2$O) at room temperature. Moreover, NaF and/or KF should be partly dissolved first and then the hexafluorostannate phases can be obtained by recrystallization in the HF solution.

Fig. 1b shows the Rietveld refinement result of the red phosphor NKSF:Mn, including the experimental and calculated patterns, the differences between the both, and the Bragg reflections of the calculated patterns. The obtained profile factors are converged to R_p = 14.30% and R_{wp} = 19.79%, which reveals a good fitting quality. The refined lattice parameters of orthorhombic NKSF are a = 11.8 Å, b = 5.995 Å, c = 8.123 Å, V = 574.6 Å^3, $\alpha = \gamma = \beta = 90°$, and space group $Pna21(33)$, which are in agreement with those in the literatures.[28,29]

Fig. 2 shows the XRD patterns of the samples obtained in 5–40 wt% HF solution with the molar ratio of NaF : KF
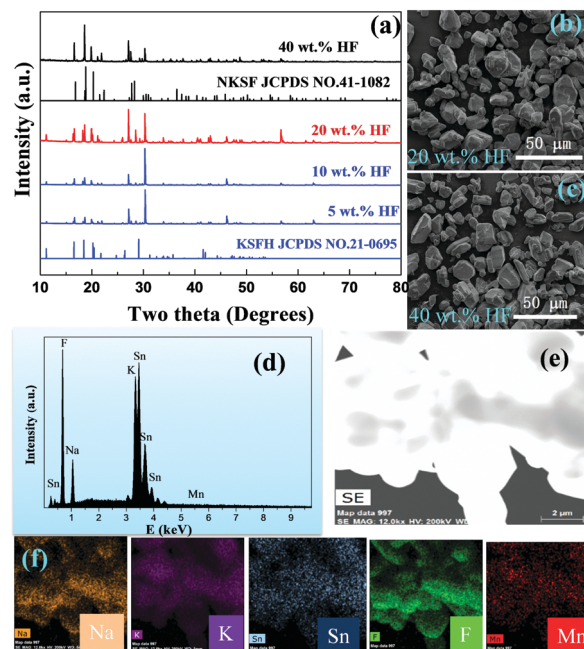
maintained at 1 : 4. The samples obtained by reactions with 5 and 10 wt% HF are probably composed of KSFH, NKSF, and KSnF$_5$ phases as shown in Fig. S1 (ESI†). The attributions for the two strong peaks at 30.4 and 46.2 degrees cannot be identified. The impurities still exist in the sample obtained in the reaction with 20 wt% HF and a pure NKSF phase can be obtained only when the HF concentration is 40 wt% HF. The results indicate that the HF concentration in the system plays a key role in the formation of a pure NKSF phase.

The microstructure and the accurate composition of the red phosphor NKSF:Mn were determined using SEM, EDS, and TEM, as shown in Fig. 2b–f. The samples obtained in 20 and 40 mol L^{-1} HF solutions show irregular morphologies with smooth surfaces and their sizes range from 5 to 20 μm (in Fig. 2b and c). The elemental composition analysis of NKSF:Mn was semi-quantitatively performed using EDS and element mapping images as shown in Fig. 2d–f. The peaks of Na, K, Sn, F, and Mn are obviously identified in the EDS spectrum of NKSF:Mn. Moreover, it is observed that the atomic percentages of Na, K, Sn, F, and Mn are approximately 12.12%, 12.20%, 12.85%, 62.31% and 0.52%, respectively, which are very close to the atomic ratio in the stoichiometric composition of NKSF:Mn. As shown in Fig. 2f, the element mapping images of Na, K, Sn, F, and Mn further confirm the composition of NKSF:Mn and indicate that the luminescence centers of Mn^{4+} ions are homogeneously dispersed in the host lattice of NKSF.

3.2. Optical properties of red phosphor NKSF:Mn

Fig. S2a (ESI†) exhibits the FTIR spectra of the samples KSF:Mn. The weak peaks at 3853 and 1589 cm^{-1} are respectively

This journal is © The Royal Society of Chemistry 2017

J. Mater. Chem. C, 2017, **5**, 9255–9263 | **9257**

attributed to the stretching and bending vibration of the O–H bond in H_2O that is attached on the surfaces of the samples. The peaks at 1218, 1184, and 728 cm^{-1} are likely due to the vibrations of the Sn–F bond in $[SnF_6]^{2-}$ groups.[20] Fig. S2b (ESI†) shows the powder diffuse reflectance spectra (DRS) of undoped NKSF and red phosphor NKSF:Mn. The spectrum of the undoped NKSF host exhibits little absorption in the range from 200 nm to 800 nm with a high reflection of about 96%. The red phosphor NKSF:Mn exhibits an absorption band at 250 nm, which is due to the charge transfer band of Mn^{4+}–O^{2-}.[15] The two absorption bands located at 378 nm and 467 nm are due to the transitions from the ground state $^4A_{2g}$ to the excited states $^4T_{1g}$ and $^4T_{2g}$ of Mn^{4+}, which indicates that the phosphor NKSF:Mn might be applied in WLEDs based on near UV and blue chips.

The excitation spectra of NKSF:Mn measured at 298 K and 78 K are shown in Fig. 3a. The two dominant excitation bands are attributed to the transitions from $^4A_{2g}$ to $^4T_{1g}$ and $^4T_{2g}$ of Mn^{4+}, respectively.[6–13] A group of sharp peaks present on the top of excitation bands ranging from 450 to 500 nm might be attributed to the scattering by excitation from a xenon lamp on the surface of crystals of micrometer size. The excitation band obtained at 78 K exhibits a blue shift compared with that measured at 298 K, which is due to the stronger crystal field splitting and the decreased vibration transition coupling associated with the vibration modes of the octahedron $[MnF_6]^{2-}$ at low temperature.[25] The excitation spectra of NKSF:Mn monitored at 627 nm, 617 nm, 612 nm, and 644 nm are shown in Fig. 3b. A blue shift is observed in both excitation bands at
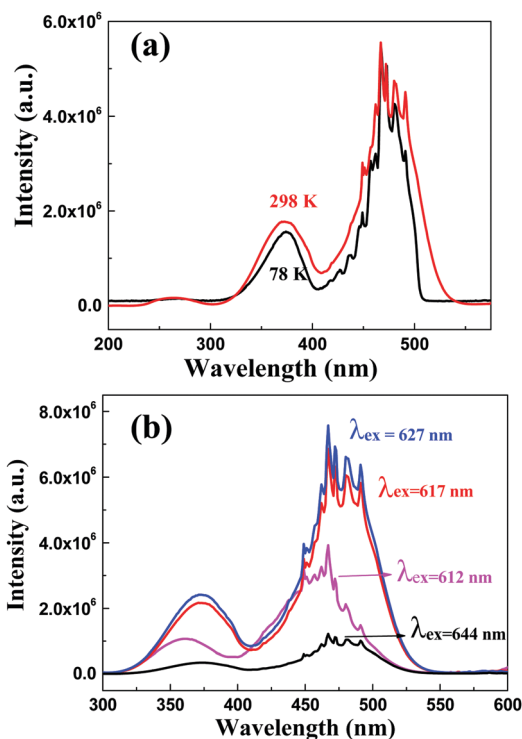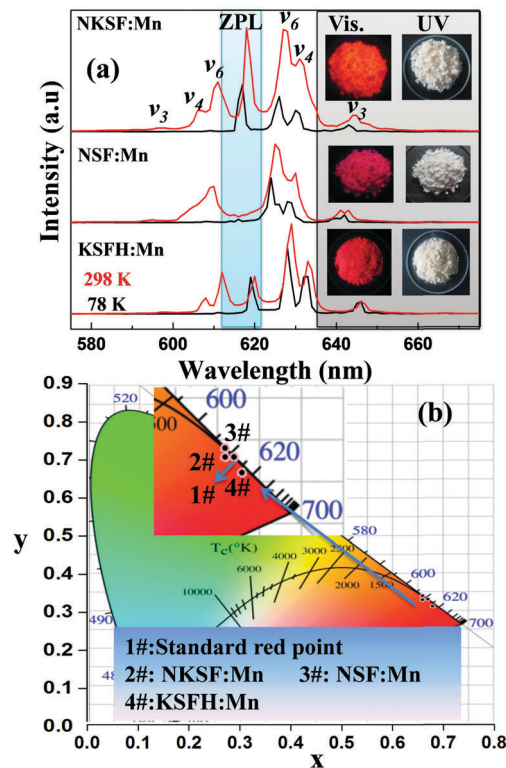
Fig. 4 (a) Emission spectra of red phosphors NaKSnF$_6$:Mn^{4+}, Na$_2$SnF$_6$:Mn^{4+}, K$_2$SnF$_6$·H$_2$O:Mn^{4+} at 78 K and 298 K, respectively, (inset: photographs of the phosphor samples under visible light and UV light), and (b) chromaticity coordinates of the three phosphors in Commission Internationale de l'Éclairage (CIE) 1931.

378 nm and 467 nm in the excitation spectrum monitored at 612 nm. This is attributed to anti-Stokes vibronic side bands associated with the excited state ^2E_g of Mn^{4+}, which disappear at 78 K (as shown in Fig. 4a).

The as-prepared powders NKSF:Mn, NSF:Mn, and KSFH:Mn are white under room light and emit intense red luminescence under a UV lamp as shown in their photographs in Fig. 4a (insert). The red phosphor NKSF:Mn exhibits a red luminescence that is more close to that of conventional red phosphor Y_2O_3:Eu than those of NSF:Mn and KSFH:Mn.[4,5] Under excitation at 467 nm, the emission spectra of samples NKSF:Mn measured at 78 K and 298 K are comparatively studied with those of NSF:Mn and KSFH:Mn as shown in Fig. 4a. The emission spectra measured at 298 K are composed of a group of sharp peaks between 600 and 650 nm.

All the emission peaks below 620 nm disappear at 78 K due to anti-Stokes vibronic side bands $\nu_3(t_{1u})$, $\nu_4(t_{1u})$, and $\nu_6(t_{2u})$ associated with the excited state ^2E_g of Mn^{4+}. The emission peaks observed at 78 K are attributed to Stokes vibronic electronic modes $\nu_6(t_{2u})$, $\nu_4(t_{1u})$, and $\nu_3(t_{1u})$ associated with transitions from ^2E_g to $^4A_{2g}$ for the 3d^3 electrons of Mn^{4+} in the octahedral environment.[15,35] The Stokes vibronic transitions of Mn^{4+} exhibit blue shifts at 78 K due the stronger crystal field at low temperature.

The Mn^{4+} ions located at the octahedral site of the hexafluorostannates are coordinated with six F$^-$ ions and substitute for $[SnF_6]^{2-}$ ions because of the same valence and the close

Fig. 3 Excitation spectra (a) measured at different temperatures and (b) monitored at different wavelengths.

9258 | J. Mater. Chem. C, 2017, 5, 9255–9263

This journal is © The Royal Society of Chemistry 2017

ionic radius of Mn^{4+} ($r = 0.530$ Å, CN = 6) and Sn^{4+} ($r = 0.605$ Å, CN = 6). The Mn^{4+} ions can stabilize in the host lattice because of the slightly smaller radius of Mn^{4+}, which facilitates the successful anion exchange between $[MnF_6]^{2-}$ and $[SnF_6]^{2-}$ ions at room temperature. It is reported that the zero photon line (ZPL) of Mn^{4+} is highly dependent on the local symmetry of Mn^{4+} surroundings.[6,17,34] Furthermore, the lower symmetry of the substituted sites in the host lattice leads to the stronger ZPL. As shown in Fig. 4a, the ZPLs are observed at 618 nm and 620 nm in the emission spectra of NKSF:Mn and KSFH:Mn, respectively. However, no ZPL is observed in the emission spectrum of NSF:Mn. This observation indicates that the crystallography environments of Mn^{4+} ions are influenced by the remote neighbouring-cations as observed in previous reports.[7,8,24] The more distortion and the lower symmetry of $[MnF_6]^{2-}$ in NKSF:Mn can generate a stronger ZPL than those in NSF:Mn and KSFH:Mn due to the partial relieving of the selection rule.[24,25] More importantly, the strong ZPL located at 618 nm in the emission spectrum of NKSF:Mn brings the CIE (Commission International de l'Eclairage 1931) coordinates of NKSF:Mn (at $x = 0.66$, $y = 0.33$) closer to the national television systems committee (NTSC) ideal red color (at $x = 0.67$, $y = 0.33$) than those of NSF:Mn (at $x = 0.68$, $y = 0.31$) and KSFH:Mn (at $x = 0.64$, $y = 0.35$), as shown in Fig. 4b. It is clearly observed that there is little absorption or emission in the range from 500 to 600 nm, which indicates that little reabsorption will occur when using the red phosphor NKSF:Mn in WLEDs with yellow phosphor YACe. Furthermore, the strong ZPL in NKSF:Mn located at 618 nm is very close to the ideal red (620 nm) in terms of the luminous efficacy of white emitting LEDs.[6]

The red phosphor NKSF:Mn shows high color purity which can be calculated by the following equation:[6,7]

$$\text{Color purity} = \frac{\sqrt{(x - x_i)^2 + (y - y_i)^2}}{\sqrt{(x_d - x_i)^2 + (y_d - y_i)^2}} \times 100\% \quad (1)$$

where (x, y) are the color coordinates of the phosphor, (x_i, y_i) are the CIE coordinates of an equal-energy illuminant with values of (0.33, 0.33), and (x_d, y_d) are the chromaticity coordinates corresponding to the dominant wavelength of the light source. The color purity is calculated to be about 99%.

3.3 Quantum yield and the optimized photoluminescence of NKSF:Mn

QY is a key parameter to evaluate a luminescent material. It is defined as the ratio of emitted photons to absorbed ones. The excitation and emission spectra of red phosphors NKSF:Mn, NSF:Mn, and KSFH:Mn measured using an integrating sphere are shown in Fig. 5. The absorbances of phosphors NKSF:Mn, NSF:Mn, and KSFH:Mn are 15.4%, 13.6%, and 47.1%, respectively, according to the following equation:[30]

$$A = \frac{L_b - L_c}{L_b} \quad (2)$$

where L_b is the integrated excitation profile when the sample is diffusely illuminated by the integrated sphere's surface;
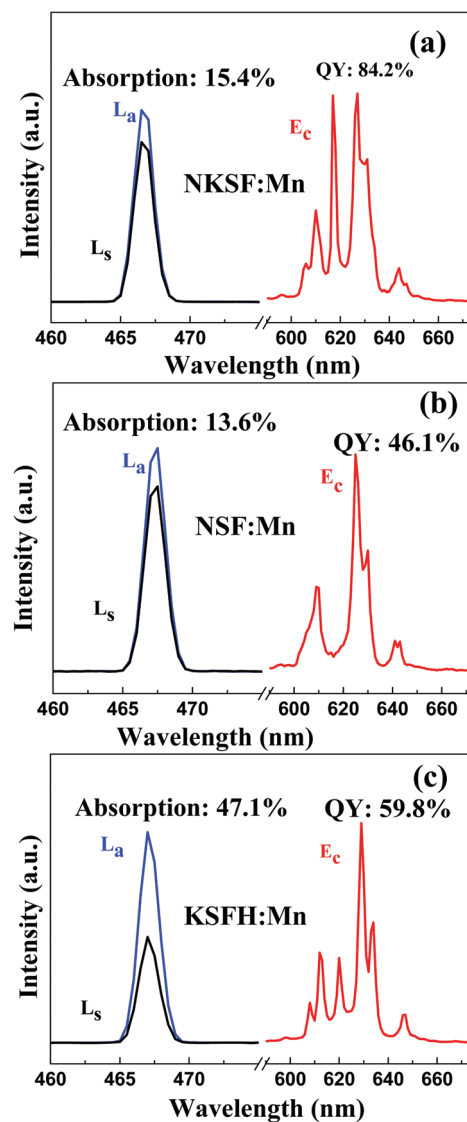

Fig. 5 The excitation lines and emission spectra of red phosphors $NaKSnF_6:Mn^{4+}$, $Na_2SnF_6:Mn^{4+}$, and $K_2SnF_6 \cdot H_2O:Mn^{4+}$ measured using an integrating sphere.

and L_c is the integrated excitation profile when the sample is directly excited by the incident beam.

The calculated internal QYs Φ_f of samples NKSF:Mn, NSF:Mn, and KSFH:Mn are 84.2%, 46.1%, and 59.8%, respectively, according to the following equation:[30]

$$\Phi_f = \frac{E_c - (1 - A) \cdot E_b}{L_a \cdot A} \quad (3)$$

where E_c is the integrated luminescence of the sample caused by direct excitation, and E_b is the integrated luminescence of the sample caused by indirect illumination from the sphere. The term L_a is the integrated excitation profile from an empty integrated sphere (without the sample). Secondary absorption and emission from the sample (that is, when the sample receives diffuse and no direct excitation light only) can be ignored. Such a case holds true with this sample, so we can ignore E_b, i.e., set equal to zero, L_b then

becomes the same as L_a. All the samples were measured using the same measurement technique under identical conditions. Thus, the results indicate that the QY of NKSF:Mn is higher than those of NSF:Mn and KSFH:Mn.

To optimize the luminescence performance of NKSF:Mn, it is necessary to investigate the influence of some general reaction parameters, such as reaction temperature and the concentration of starting materials on its photoluminescence properties. Fig. S3 (ESI†) shows that the pure NKSF phase can be easily obtained from room temperature to 160 °C and the concentration of K_2MnF_6 has little influence on the crystallization of the NKSF phase.

It is observed that the emission intensity is strongly dependent on the reaction temperature and the concentration of K_2MnF_6. Fig. 6a shows that the features and location of emission spectra remain constant when the samples are prepared at various temperatures and the strongest integrated emission intensity is obtained at 80 °C. Compared with heating at 25 °C, heating at 80 °C can increase the exchange interaction probability between anions $[MnF_6]^{2-}$ and $[SnF_6]^{2-}$, which facilitates the formation of luminescence centers. Moreover, the solubility of two fluorides NKSF and K_2MnF_6 in HF solution increases with increasing temperature which is favorable for the entrance of Mn^{4+} into the host lattice.[8] Whereas the luminescence intensity

decreases dramatically when the temperature is increased to 120 or 160 °C. This is probably due to decomposition of K_2MnF_6 at elevated temperature, resulting in the lower number of Mn^{4+} ions entering the crystal lattice.[11,36]

It can be clearly observed in Fig. 6b that all the emission spectra are of similar shape. With increasing K_2MnF_6 concentration, the emission intensity of NKSF:Mn increases. When the molar ratio of K_2MnF_6 to NKSF is 1.0 mol%, the as-obtained sample NKSF:Mn shows the strongest emission intensity. With a continuous increase of K_2MnF_6 concentration, the emission intensity decreases, which is due to the concentration quenching of Mn^{4+} in the NKSF crystal lattice. It should be noted that the actual concentration of Mn^{4+} in the crystallized fluoride samples is dependent on the solubility of K_2MnF_6 and the host lattice of fluorides in HF solution. As measured by the inductively coupled plasma-atomic emission spectroscopy (ICP-AES) analysis and X-ray photoelectron spectroscopy (XPS) in reactions for synthesizing red phosphor K_2TiF_6:Mn^{4+}, there were 32.4 mol% of manganese entering the crystal lattices and 67.6 mol% were left in the filtrate.[14] Thus, the actual doping concentration of Mn^{4+} in the fluoride phosphors is generally lower than the molar ratio of the starting materials K_2MnF_6 to host lattice of fluorides.

The decay curves of 627 nm emission (excited at 467 nm) of a series of red phosphors NKSF:Mn with different concentrations of K_2MnF_6 were examined at room temperature (as shown in Fig. 7a). These curves can be fitted into a single-exponential function, and their lifetime values are 2.60–3.46 ms as the concentration of K_2MnF_6 increases from 0.05 to 16.0 mol% of NKSF. The lifetime decreases with the concentration of K_2MnF_6 due to the increase in the exchange interaction probability between Mn^{4+} ions. The decay curves are also strongly dependent on the measurement temperature as shown in Fig. 7b. The decay time at 78 K is 3.91 ms which is longer than that measured at 298 K (3.24 ms). The decrease of lifetime of ^2E_g–$^4A_{2g}$ with increasing temperature results from the opening of additional relaxation pathways with increasing temperature.[24]

3.4 Thermal stability of phosphor NKSF:Mn

Since the fabrication and working temperature of LEDs is around 150 °C, the thermal stability and the temperature dependence on the luminous efficiency are important parameters for phosphors.[31] To study the thermal stability of the as-prepared red phosphor NKSF:Mn, the TGA-DSC curves are obtained by heating the sample in the temperature range of 35–1000 °C with a heating rate of 10 °C min^{-1} in a nitrogen atmosphere. The TGA results reveals that the total weight loss is 1.5% up to 420 °C accompanied by three exothermic peaks, which can be attributed to the removal of absorbed moisture. The large and sharp exothermic DSC peak and dramatic loss of weight indicate that NKSF:Mn starts to decompose around 450 °C. The thermal quenching properties of the NKSF:Mn phosphor in the temperature ranging from room temperature to 300 °C are depicted in Fig. 8b. It can be clearly observed that the emission intensity exhibits a decreasing trend with the temperature increasing because of the increasing nonradiative transition processes induced by unit cell expansion and vibration probability enhancement under heat treatment.[6,22,24]
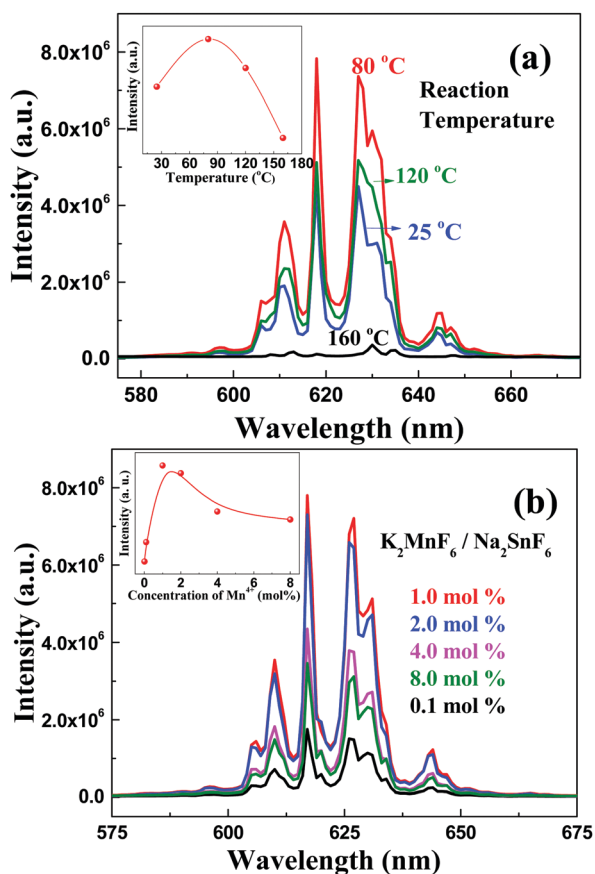

Fig. 6 Emission spectra, and integrated luminescence intensity of NaKSnF$_6$:Mn^{4+} dependent on (a) reaction temperature and (b) the concentration of K_2MnF_6.
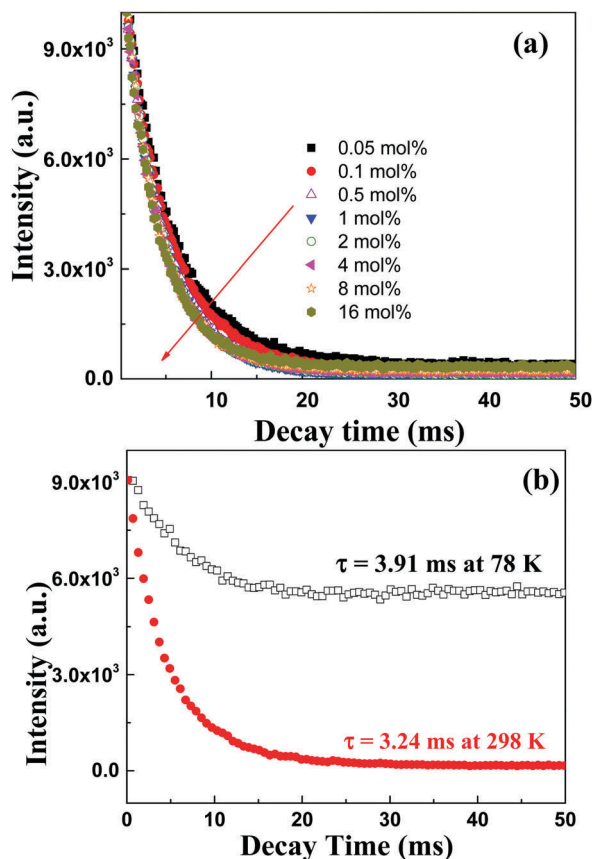
9260 | *J. Mater. Chem. C*, 2017, **5**, 9255–9263

This journal is © The Royal Society of Chemistry 2017

Fig. 7 Decay time for red emission of NaKSnF$_6$:Mn^{4+} dependent on the concentration of K$_2$MnF$_6$ and the measurement temperature.

Fig. 8 (a) TG and DSC curves of red phosphor NaKSnF$_6$:Mn^{4+}, (b) the integrated luminescence intensity varies with measurement temperature. (Inset: Arrhenius fitting of the integrated luminescence intensity decreased with increasing temperature.)

To evaluate the influence of temperature on the luminescence, we use the following Arrhenius equation to calculate the activation energy E_a of NKSF:Mn:[32,33]

$$I_T = \frac{I_0}{1 + c \exp\left(-\dfrac{E_a}{kT}\right)} \qquad (4)$$

where I_0 is the initial luminescence intensity of NKSF:Mn at room temperature, I_T is the luminescence intensity of NKSF:Mn at different temperatures, c is a constant, E_a is the activation energy, and k is the Boltzmann constant. The activation energy E_a can be calculated by plotting $\ln[(I_0/I_T) - 1]$ against $1/k_T$ as shown in the inset of Fig. 8b. The slope of the fitting line that is equal to E_a is 0.3084 eV.

3.5 Application of NKSF:Mn in warm WLEDs

Due to the superior luminescence performances of NKSF:Mn, the as-obtained red phosphor NKSF:Mn was fabricated on the GaN chip (with blue emission at around 460 nm and a luminous efficacy higher than 137 lm W^{-1}) with commercial yellow phosphor YAG:Ce. The photographs of WLEDs exhibit cold and warm white light in the absence and presence of NKSF:Mn (in Fig. 9a and b), respectively. As shown in Fig. 9c, the electroluminescence spectra of WLEDs show a broad band in the blue regi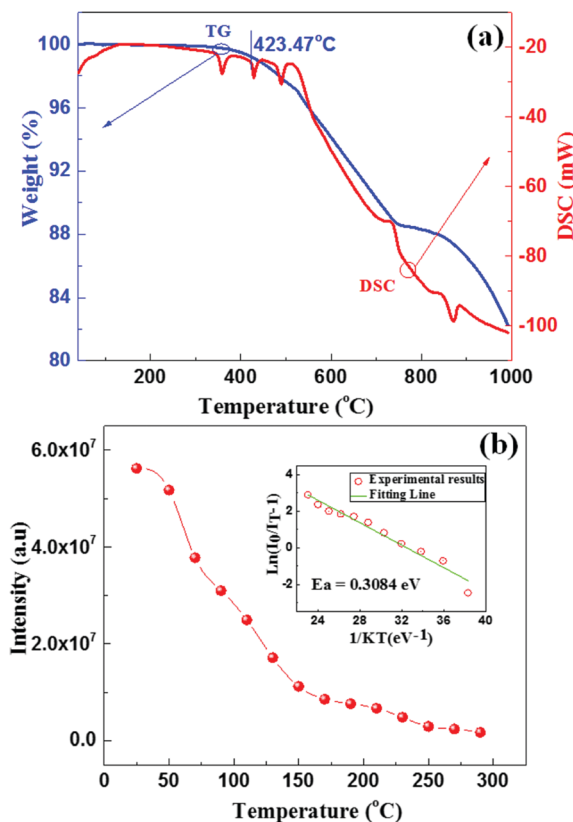on due to the emission of the GaN chip and a yellow emission that is due to the emission of YAG:Ce without mixing the red phosphor NKSF:Mn. A group of peaks in the red region shown in the spectrum in Fig. 9d are attributed to the spin-forbidden ^{2}E$_g$–^{4}A$_{2g}$ transitions of Mn^{4+} ions from NKSF:Mn, which indicates that the phosphor NKSF:Mn can absorb the electroluminescence of a GaN chip and covert it to an intense red light. As shown in Fig. 9e and f, the obtained white light exhibits weak emission in the red region with a CRI of 61.1 at CCT = 6281 K when only a single YAG:Ce phosphor is provided for luminescence conversion. After the addition of NKSF:Mn, the CRI increases to 90.4 and the CCT decreases to 3746 K, and a warm white light with chromaticity coordinates (0.33, 0.34) is obtained under a driven current of 30 mA. The results reveal that NKSF:Mn presents good luminescence properties and could be a candidate material for use in backlighting systems with warm white light.

4. Conclusions

In conclusion, we obtained a red fluoride phosphor NKSF:Mn at room-temperature. We found that the concentration of HF and the ratio of NaF to KF are significant for the formation of NKSF rather than NSF or KSFH. The chromaticity coordinates for phosphor NKSF:Mn are located at $x = 0.66$ and $y = 0.33$, which are very close to the CIE coordinates of the ideal red

This journal is © The Royal Society of Chemistry 2017

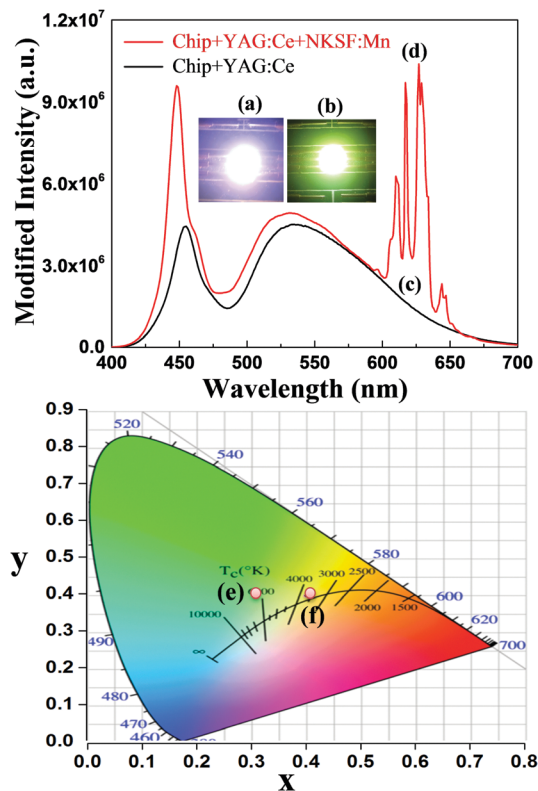*J. Mater. Chem. C*, 2017, **5**, 9255–9263 | **9261**

Fig. 9 (a and b) The images and (c and d) electroluminescence spectra, and (e and f) chromaticity coordinates of two WLEDs with the blue GaN chip, yellow phosphor YAG:Ce^{3+} (a, c and e) without and (b, d and f) with a red phosphor NaKSnF$_6$:Mn^{4+}.

region (0.67, 0.33) due to the contribution of particularly strong zero-phonon lines at 618 nm. The internal QY of the phosphor NKSF:Mn is 84%, which is higher than those of the phosphors NSF:Mn and KSFH:Mn. In comparison to NKSF:Mn prepared at 80 °C, the samples NKSF:Mn obtained at a higher temperature show lower luminescence intensity, which may be attributed to the decomposition of K$_2$MnF$_6$. The optimal concentration of K$_2$MnF$_6$ in the reaction system is 1.0 mol% of NKSF. The red phosphor NKSF:Mn can be a good candidate for application in GaN–YAG:Ce type LEDs for obtaining a warm white light.

Conflicts of interest

There are no conflicts to declare.

Acknowledgements

References

1 H. S. Jang, Y.-H. Won and D. Y. Jeon, *Appl. Phys. B: Lasers Opt.*, 2009, **95**, 715–720.

2 C. Feldmann, T. Jüstel, C. R. Ronda and P. J. Schmidt, *Adv. Funct. Mater.*, 2003, **13**, 511–516.

3 H.-D. Nguyen, C. C. Lin and R. S. Liu, *Angew. Chem., Int. Ed.*, 2015, **54**, 10862–10866.

4 A. V. Murugan, A. K. Viswanath, V. Ravi, B. A. Kakade and V. Saaminathan, *Appl. Phys. Lett.*, 2006, **89**, 123120.

5 J. G. Li, X. Li, X. Sun and T. Ishigaki, *J. Phys. Chem. C*, 2008, **112**, 11707–11716.

6 E. H. Song, J. Q. Wang, S. Ye, X. F. Jiang, M. Y. Peng and Q. Y. Zhang, *J. Mater. Chem. C*, 2016, **4**, 2480–2487.

7 Y. W. Zhu, L. Huang, R. Zou, J. H. Zhang, J. B. Yu, M. M. Wu, J. Wang and Q. Su, *J. Mater. Chem. C*, 2016, **4**, 5690–5695.

8 Y. W. Zhu, L. Y. Cao, M. G. Brik, X. J. Zhang, L. Huang, T. T. Xuan and J. Wang, *J. Mater. Chem. C*, 2017, **5**, 6420–6426.

9 S. Adachi and T. Takahashi, *J. Appl. Phys.*, 2008, **104**, 023512.

10 X. Q. Li, X. M. Su, P. Liu, J. Liu, Z. L. Yao, J. J. Chen, H. Yao, X. B. Yu and M. Zhan, *CrystEngComm*, 2015, **17**, 930–936.

11 L. Huang, Y. W. Zhu, X. J. Zhang, R. Zou, F. J. Pan, J. Wang and M. M. Wu, *Chem. Mater.*, 2016, **28**, 1495–1502.

12 M. Kim, W. B. Park, B. Bang, C. H. Kim and K. S. Sohn, *J. Am. Ceram. Soc.*, 2017, **100**(3), 1044–1050.

13 M. Kim, W. B. Park, B. Bang, C. H. Kim and K. S. Sohn, *J. Mater. Chem. C*, 2015, **3**, 5484–5489.

14 L. F. Lv, Z. Chen, G. K. Liu, S. M. Huang and Y. X. Pan, *J. Mater. Chem. C*, 2015, **3**, 1935–1941.

15 H. M. Zhu, C. C. Lin, W. Luo, S. Shu, Z. Liu, Y. Liu, J. Kong, E. Ma, Y. Cao, R. S. Liu and X. Y. Chen, *Nat. Commun.*, 2014, **5**, 4312.

16 X. Y. Jiang, Z. Chen, S. M. Huang, J. G. Wang and Y. X. Pan, *Dalton Trans.*, 2014, **43**, 9414–9418.

17 Y. Arai, T. Takahashi and S. Adachi, *Opt. Mater.*, 2010, **32**, 1095–1101.

18 R. Hoshino and S. Adachi, *Opt. Mater.*, 2015, **48**, 36–43.

19 Y. Arai and S. Adachi, *J. Lumin.*, 2011, **131**, 2652–2660.

20 L. Q. Xi, Y. X. Pan, X. Chen, S. M. Huang and M. M. Wu, *J. Am. Ceram. Soc.*, 2017, **100**, 2005–2015.

21 Q. Zhou, H. Y. Tan, Y. Y. Zhou, Q. H. Zhang, Z. L. Wang, J. Yan and M. M. Wu, *J. Mater. Chem. C*, 2016, **4**, 7443–7448.

22 R. Kasa and S. Adachi, *J. Appl. Phys.*, 2012, **112**, 013506.

23 Y. K. Xu and S. Adachi, *J. Appl. Phys.*, 2009, **105**, 013525.

24 W. L. Wu, M. H. Fang, W. Zhou, T. Lesniewski, S. Mahlik, M. Grinberg, M. G. Brik, H. S. Sheu, B.-M. Cheng, J. Wang and R.-S. Liu, *Chem. Mater.*, 2017, **29**, 935–939.

25 L. L. Wei, C. C. Lin, Y. Y. Wang, M. H. Fang, H. Jiao and R. S. Liu, *ACS Appl. Mater. Interfaces*, 2015, **7**, 10656–10659.

26 Q. Zhou, Y. Y. Zhou, Y. Liu, L. J. Luo, Z. L. Wang, J. H. Peng, J. Yan and M. M. Wu, *J. Mater. Chem. C*, 2015, **3**, 3055–3059.

27 K. O. Christe, *Inorg. Chem.*, 1986, **25**, 3721–3722.

28 T. F. Antokhina, S. B. Ivanov, N. N. Savchenko and L. V. Teplukhina, *Biol. Bull. Acad. Sci. USSR*, 1987, **36**, 1785–1789.

29 E. F. Schubert, T. Gessmann and J. K. Kim, *Kirk-Othmer Encycl. Chem. Technol.*, John Wiley & Sons, Inc., 2000, DOI: 10.1002/0471238961.1209070811091908.a01.pub2.

30 Integrating Sphere F-3018 Operation Manual Part number 81089 version 1.1, provided by HORIBA Jobin Yvon Inc., May, 2005.

31 H. Wang, P. He, S. Liu, J. Shi and M. Gong, *Appl. Phys. B: Lasers Opt.*, 2009, **97**, 481.

32 Z. G. Xia, X. M. Wang, Y. X. Wang, L. B. Liao and X. P. Jing, *Inorg. Chem.*, 2011, **50**, 10134–10142.

33 B. Henderson and G. F. Imbusch, *Optical Spectroscopy of Inorganic Solids*, Clarendon Press, Oxford, 1989.

34 Y. K. Xu and S. Adachi, *J. Appl. Phys.*, 2009, **105**, 013525.

35 E. H. Song, J. Q. Wang, J. H. Shi, T. T. Deng, S. Ye, M. Y. Peng, J. Wang, L. Wondraczek and Q. Y. Zhang, *ACS Appl. Mater. Interfaces*, 2017, **9**, 8805–8812.

36 S. Adachi and T. Takahashi, *J. Appl. Phys.*, 2009, **106**, 013516.